Design and Analysis of a Rotational Mixer to produce 3D Bioprinting Gyroid-Helical-Patterned Scaffolds for Tissue Engineering Applications

Mariana S. Flores-Jiménez [1], Rita Q. Fuentes-Aguilar [2*] and Alejandro Garcia-Gonzalez [3], Member, *IEEE*

***Abstract*— Tissue engineering scaffolds require complex networks for nutrient diffusion and cell attachment. They must have specific surface area and curvature, and often need a multimaterial composition, demanding advanced micro-fabrication methods. 3D extrusion bioprinting offers versatility to manufacture different scaffold, and strategies for multimaterial printing have been introduced. We propose a method to fabricate scaffolds based on gyroid-helical-patterned microfibers, providing a platform to study the effect of the gyroid minimum curvature on cellular processes, since the geometry wont be layer-by-layer approximated. The pattern is obtained by mixing inks using a gyroid-helix shaped rotational mixer, modifying the extruder of a conventional 3D printer. The mixer was simulated using computational fluid dynamics tools, varying the volumetric flow to obtain different gyroid-thickness. Due to its surface area minimization, it shows lower energy requirements than state-of-art fluid mixers, with a pressure drop of 1.7%, a power number of 39, and a rotation-induced shear stress of ∼400 Pa, enabling the use of cell-embedded bioinks.**

I. INTRODUCTION

Complex architectures for tissue scaffolds are needed to mimic the networks and patterns present in multiple tissues [1], [2]. Recent research has been focused on 3D printing scaffolds based on the extrusion of non-cylindrical strands, using distinct nozzle shapes [3], or employing a rotational nozzle to extrude multimaterial helical filaments [4]. The curvature control of these filaments could give us a platform to study cell curvature-driven processes, mainly in little explored geometries, such as the gyroid, a minimal surface with no self-intersections, negative Gaussian curvature and zero mean curvature, properties identified in energy-minimizing tissue formation, cell migration, cytoskeleton orientation and at arteries bifurcation [5]. Gyroid-based scaffolds have been fabricated using stereolitography (SLA) with a 25 μm layer thickness [6], selective laser sintering (SLS) for pore diameters of 200 to 1200 μm [7], and digital light processing (DLP) for a layer thickness of 84 μm [8], and 282 μm [9]. Also by mold casting, with a pore diameter of 1 mm [10], and by 3D printing, using a highly viscous self-supported ink, resulting in a gyroid cubic cell of 15 mm^3 [11]. These approaches have limitations regarding the availability of photosensitive resins, low biocompatibility, large periods of fabrication, low versatility due to molds delimitation, lack of surface smoothness because layer-by-layer approximation, and resolution dependency on nozzle diameter, where the smallest is commonly around 100 μm. This hinders the cells to take advantage of the gyroid's real curvature, since the substrate curvature radii have an effect on collective cell behavior if they are in the range of 5 to 9 cell lengths [12]. This work proposes the incorporation of a rotational mixer, based on the helical chirality of the gyroid, into a 3D extrusion printing system, using low-viscosity hydrogels. In this way, extruding helical-gyroid-micro-patterned filaments form different lattices. This methodology can be adapted to the sheet or skeletal gyroid, and the surface curvature will no longer be dependent on the layer thickness conferred by the nozzle diameter since the helix will be embedded in a continuous strand. Two or more inks can be used to form multicellular fiber, as well as sacrificial materials, to obtain hollow helical fibers. We simulated the mixer in a computational fluid dynamics (CFD) tool and we compare it with the Kenics static mixer (KSM).

II. METHODOLOGY

A. Mixer Design

The gyroid is chiral in local helices along the crystallographic planes (100), (110), (111) [13], as shown in Fig. 1a). We designed a mixer, based on these helices, to obtain an output pattern that could be rotated to form the gyroid-helical part, as illustrated in Fig. 1b-c). In specific, the right-handed helix (RHH) in plane (100), void centered, was selected, but left-handed helix (LHH) can also be formed by changing the direction of rotation.

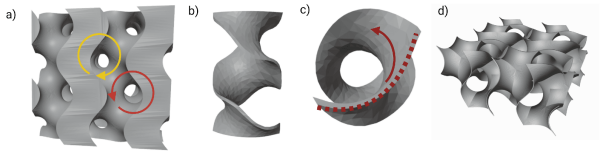

Fig. 1. a) Skeletal Gyroid projected in crystallographic plane (100), highlighting RHH and LHH void centered. b) RHH lateral view. c) RHH top view, highliting the pattern to be rotated. d) Gyroid in a sheet configuration.

The gyroid-helical mixer (GHM) was designed to be inside of a 3 ml syringe with an internal diameter of 8.4 mm, but was considered 8.2 mm to avoid friction. The thickness was calculated based on the proportion $0.04 * diameter$, the same as for Kenics static mixers (KSM), since they have been

*This work was supported by Intel Rise ID 78663 and Tecnológico de Monterrey

[1] M.F. is with Escuela de Ingeniería y Ciencias, Tecnológico de Monterrey Campus Guadalajara, Av Gral. Ramon Corona No 2514, Zapopan, Jalisco, Mexico

[2] R.F. is with the Institute of Advanced Materials for Sustainable Manufacturing, Tecnológico de Monterrey Campus Guadalajara, Av Gral. Ramon Corona No 2514, Zapopan, Jalisco, Mexico rita.fuentes@tec.mx

[3] A.G. is with Escuela de Medicina y Ciencias de la Salud, Tecnológico de Monterrey Campus Guadalajara, Av Gral. Ramon Corona No 2514, Zapopan, Jalisco, Mexico

explored for bioprinting multilayered fibers [14], and thus, marking a starting point for our research. The GHM length was the same as the gyroid cubic cell length, to preserve the minimal surface proportions. The GHM can be adapted to fabricate helices based on the skeletal or sheet gyroid-based geometry. They can be differentiated in Fig. 1a) and d).

B. Fluid Flow Calculations

We considered the hydrogel flow from the syringe to a conical nozzle, using 1 to calculate the volumetric flow Q in the nozzle [15],

$$Q = \frac{\pi D_i^3 D_o^3}{32}\left(\frac{3n\Delta P tan\theta_c}{2K(D_i^{3n} - D_o^{3n})}\right)^{1/n}, \quad (1)$$

where ΔP is the pressure drop, D_i is the inlet diameter of the conical nozzle and D_o the diameter at the exit, θ_c is the half cone angle, and K and n describe the fluid viscosity in terms of the power law. Q is the sum of the volumetric flow of each channel created by the mixer (Q_i). The gyroid separates the space into two equal-volume domains, therefore, the transversal areas of the channels are the same, and they both contribute equally to Q. However, a gyroid family of constant mean curvature (CMC) can be obtained by surface deformations, enclosing a volume not equal to 50% [13]. In that case, Q_i will not be the same for each channel, each one will be proportional to the volume that encloses. In [16], we parameterized the gyroid deformation using 2, establishing a relationship between the enclosed volume, or porosity (p), and a deformation variable δ, which is also equivalent to the gyroid thickness,

$$\delta = \frac{(0.786p^3 - 1.179p^2 - 2.529p + 1.4597) * 0.3}{1.5}. \quad (2)$$

C. Simulation as Static Mixer

We first simulate the GHM as a static mixer to confirm the mixing pattern and to compare its performance, in terms of pressure drop and mixing energy, with the KSM and with a mixer based on gyroid's complete cubic cell, reported in [17]. The pressure drop was used as an indicator of the flow obstruction by the mixer, while the mixing energy was characterized in terms of the dimensionless power number k_p, as in 3, to analyze the energy requirements,

$$k_p = \left(2 * \frac{\Delta P}{2\rho u^2}\frac{4V_s}{A_s L}\right) * Re, \quad (3)$$

where ΔP is the pressure drop, ρ the fluid density, u the mean flow velocity, L the mixer length, V_s the mixer volume, A_s the mixer surface area, and Re is the Reynolds number.

The simulation was performed in COMSOL Multiphysics 5.5 ®, using the Laminar Flow module and a stationary solver. We simulate a 4% w/v alginate ink, the density was 1052.94 kg m^{-3}, and fluid viscosity was established with power law values $n = 0.930$ and $K = 0.7028$ Pa·s [18]. Fully developed flow and no-slip boundary conditions were established, with an extra-fine triangular mesh. The inlet was divided with the shape of the channels created by the GHM. To observe the mixing pattern, the Particle Tracing Module was used with a time-dependent solver and a freeze boundary condition at the output, tracking 10^5 massless particles.

D. Mixer Setup in 3D Extrusion Printer

To obtain the complete gyroid-helical pattern, the output of the GHM should be rotated. The nozzle can be rotated as in [4], however, that mechanism limits us to one nozzle size. We propose to rotate the GHM, enabling the exchange of the nozzle, and allowing the gyroid-helix diameter variation. The rotational mechanism was adjusted to a conventional 3D printer with piston-driven dispensing. A screw parallel co-rotation system was adapted to attach the GHM, as shown in Fig. 2a). We didn't need any external motor or control device, and the GHM rotation was synchronized to the *gcode* that the printer follows to fabricate a complete lattice. Syringe pumps were adapted to feed the inks at the inlets of the GHM, as illustrated in Fig. 2b).

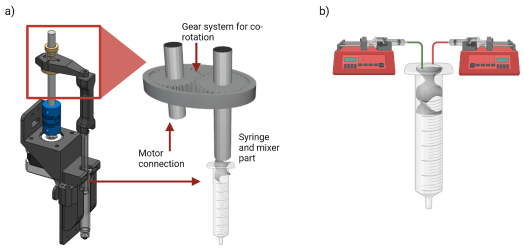

Fig. 2. a) The extruder of a Wanhao Duplicator i3 3D printer, previously modified, was replaced by a gear co-rotation mechanism for the GHM rotation. b) The inks are fed to the GHM inlets through syringe pumps.

Since the rotation was intended to serve as an output pattern changer, it was necessary for the rotational velocity to be coordinated with Q. For a gyroid cubic cell, the helix length (h_l) is twice the helix diameter (h_d), so, for a nozzle with a $D_o = 0.250$ mm, $h_d = 0.250$ mm and $h_l = 0.5$mm. From this, the volume of the filament (V_f) needed to be extruded, to form the helical-gyroid pattern, was obtained. The time needed to extrude that volume (t_v), depended of Q, as $t_v = V_f/Q$, and that was the same time for the GHM to do a revolution.

E. Mixer Simulation as Rotating Machinery

The shear stress, generated at the GHM walls due to the rotation, was also simulated in COMSOL using the Rotating Machinery for Laminar Flow module, with a time-dependent solver and a moving mesh, using the same settings established for static simulation. The KSM rotation was also simulated for comparison.

F. 3D Bioprinting and cell viability test

The GHM was used to extrude two inks, one to serve as the main structure and the second to be the sacrificial material. The first one, AG, was composed of 4% (w/v) sodium alginate (Sigma-Aldrich) and 7% (w/v) gelatin (porcine skin type A, Sigma-Aldrich). The second ink was Carbopol 980 (Abreiko). The AG ink was crosslinked with $CaCl_2$ 100mM,

which also dissolved the Carbopol. They were extruded at room temperature with plastic tapered nozzles with an internal diameter of 1.5 mm and 3 mm. A GHM with 0.328 mm thickness and skeletal configuration was used. The corresponding flow rate was calculated as previously described. A cell viability test was performed to check the survival percentage of the cells embedded in the AG ink. For this, a live/dead kit (Thermo-Fisher) and a Zeiss Zen LSM800 confocal microscope were used.

III. RESULTS

A. Mixer Design

The GHM inserted in a syringe with a conical tip is illustrated in Fig. 3a). The GHM thickness resulted in 0.328 mm, equal to a δ of 0.04, as shown in Fig. 3b) For the skeletal configuration, this thickness, according to 2, corresponds to a porosity, or a pore channel proportion C_p, of 43.53%, and solid volume, or solid channel proportion C_s, of 56.47%. This relation can be inverted according to the application and use of structural and sacrificial inks. For the sheet configuration, the total thickness was duplicated, that is, the central channel measures 0.336 mm, and each wall 0.168 mm, giving a total thickness of 0.672 mm, corresponding to δ of 0.08. The solid volume is equivalent to the volume of the central channel, while the pore volume corresponds to the outside channels, which have a proportion of $C_{p1} = 37.07\%$ and $C_{p2} = 62.93\%$, as shown in Fig. 3b).

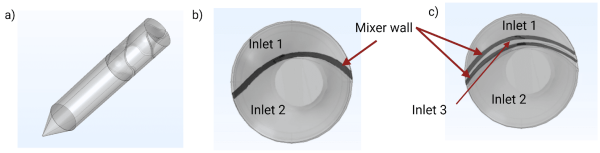

Fig. 3. a) GHM inserted in a 3 ml syringe with a conical nozzle of $D_o = 0.250$ mm. b) Two inlets, or channels, are formed using a GHM in a skeletal configuration. c) Three inlets, or channels, are formed using a GHM in a sheet configuration.

B. Fluid Flow and Simulation as Static Mixer

According to 1, the flow rate for a conical nozzle with $D_o = 0.250$ mm, is of 0.182 mm^3/s, implicating a pressure of 60 Pa at the nozzle. The δ deformation gives us the ratio to calculate the total Q. For example, for a porosity of 50% in a skeletal configuration, Q should be divided in both channels to form a pore volume, V_p, equal to the solid one, V_s, but as we have one channel bigger, it should be adjusted as $Q_s = \left(Q * \frac{V_s}{100}\right) * \left(\frac{|C_s - V_s|}{V_s} + 1\right)$ and $Q_p = \left(Q * \frac{V_p}{100}\right) * \left(1 - \frac{|C_p - V_p|}{V_p}\right)$. The variation of patterns at the nozzle output, due to changes in Q_s and Q_p, are shown in Fig. 4a-d). For the sheet configuration, it has to be considered the addition of the central channel flow, which corresponds to Q_s, and Q_p should be adjusted to the outside channels proportions C_{p1} and C_{p2}. The different outputs for this configuration are shown the Poincare maps in Fig. 4e-h).

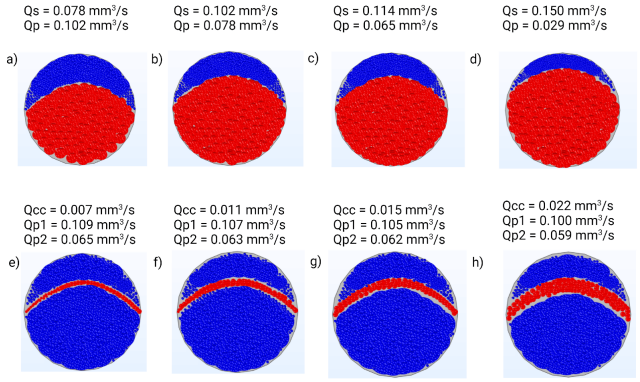

Fig. 4. a)-d) Patterns for skeletal configuration. Blue is for pore volume and red is for solid. Pore volume decreased as Q_s increased. e)-h) Patterns for sheet configuration. The thickness of the central channel increased as Q_s increased.

The pressure drop and shear stress at the GHM walls, considering the dynamic viscosity of the 5% alginate and $Q = 0.182$ mm^3/s, are observed in Fig. 5. The pressure drop is of 1.7% and the shear stress is below 5 Pa.

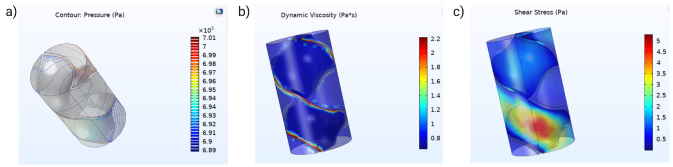

Fig. 5. a) Pressure drop in the mixer section. b) Dynamic viscosity. c) Shear stress that the fluid experiences at the mixer wall.

In [17], authors reported the simulation of a KSM and a gyroid cubic cell mixer (GCCM). They indicated that the GCCM had a better energy performance than the KSM due to the zero mean curvature and higher hydraulic diameter. The power number, k_p, was ∼200 for KSM and ∼130 for the gyroid. A second simulation for the GHM, using water and the same Q as in the article, gives us a k_p of 39, making it the mixer with the lowest energy requirement, since the minimal area avoids the loss of energy by friction. The pressure drop for the GHM with these conditions resulted in 1.92%, which indicates that its geometry allows smooth flow transition.

C. Mixer Simulation as Rotating Machinery

For Q of 0.182 mm^3/s, the GHM should give a revolution in 0.5 s to extrude a complete gyroid-helix. The shear stress on the walls remains constant during rotation for both mixers. For the KSM, the highest value is registered at the top and bottom corners, while for the GHM, the highest values are at the lateral edges, but they are lower than those of the KSM. The maximum for KSM is ∼ 450 Pa, and for GHM is ∼ 400 Pa. After rotating the output, the helix can be formed within the filaments that are being extruded, giving the possibility of fabricating scaffolds based on different lattices with the gyroid-helices embedded, as illustrated in Fig. 6a). Even a complete gyroid cubic cell can be formed by following the direction and screw axes of the helices, as shown in Fig. 6b).

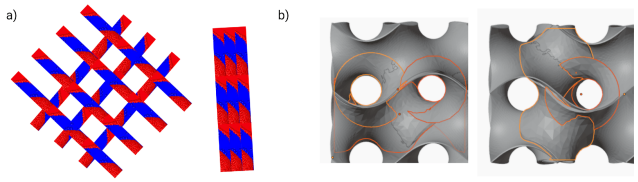

Fig. 6. a) Filaments arranged to form squared-based scaffolds. b) Gyroid cubic cell with the chiral helices embedded.

D. 3D Bioprinting and cell viability test

The results after the extrusion of the AG and Carbopol inks are shown in Fig. 7. The filament with the mixing pattern is shown in Fig. 7 a), while Fig. 7 b), shows the resulting structure after the Carbopol removal. A 99% viability after 24h can be observed in Fig. 7 c), and Fig. 7 d) shows a 3D reconstruction of the position of the cell in a 600x600x200 μm section of the AG part bioprinted with the smallest nozzle.

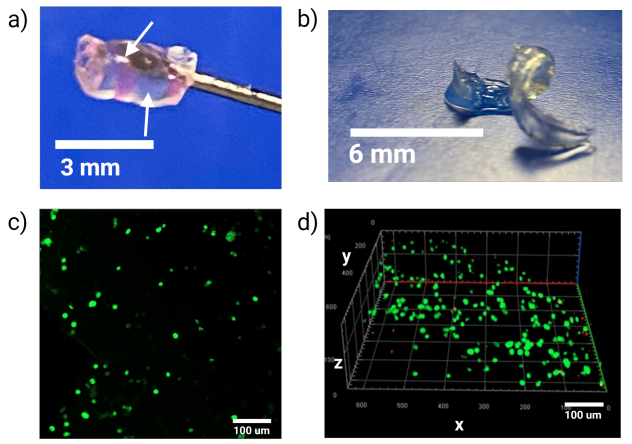

Fig. 7. a) Mixed filament. The arrows point at different materials, (pink is for Carbopol and light blue is for AG). b) AG structure after Carbopol removal. c)2D slice at the middle of the AG structure. d) 3D confocal microscope image reconstruction.

IV. CONCLUSION

The proposed 3D extrusion bioprinting method, for gyroid-helical-patterned microfibers, intends to be an advanced manufacturing technique for complex tissue scaffolds, solving limitations regarding interconnecting networks and curved surfaces. The main advantages lie in resolution improvement, surface smoothing, and preservation of the gyroid's curvature. Compared to conventional 3D bioprinting, a 90% size reduction is obtained, and the nozzle is interchangeable to vary gyroid-helix size. The use of GHM was validated through CFD simulations, proving its versatility to form gyroid-helical fibers with a sheet or skeletal configuration, and obtaining different thicknesses and patterns just by varying the volumetric flow. More inks can be used, by introducing more channels in parallel, similar to the sheet-based GHM. The energy requirements of the GHM are lower than those of other fluid mixers, and it presents a low rotational-induced shear stress of 400 Pa.

ACKNOWLEDGMENT

M.F. acknowledges a Ph.D. stipend from CONACYT and Tecnologico de Monterrey. A.G. acknowledges the Diagnostic and Therapeutic Innovation in Chronic Degeneration Diseases group. R.F. acknowledges Advanced Cyberphysical Systems Laboratory.

REFERENCES

[1] L. Shao, Q. Gao, H. Zhao, C. Xie, J. Fu, Z. Liu, M. Xiang, and Y. He, "Fiber-Based Mini Tissue with Morphology-Controllable GelMA Microfibers," *Small*, vol. 14, Nov. 2018.

[2] Flores-Jiménez, Mariana S and Garcia-Gonzalez, Alejandro, and Fuentes-Aguilar, Rita Q, "Review on Porous Scaffolds Generation Process: A Tissue Engineering Approach", *ACS Applied Bio Materials*, ACS Publications, 2023.

[3] Y. Raymond, E. Thorel, and M. Ginebra, "3D printing non-cylindrical strands: Morphological and structural implications," *Additive Manufacturing*, vol. 46, Oct. 2021.

[4] N. Larson, J. Mueller, A. Chortos, Z. Davidson, D. Clarke, and J. Lewis, "Rotational multimaterial printing of filaments with subvoxel control," *Nature*, vol. 613, Jan. 2023, pp. 682-688.

[5] S. Callens, R. Uyttendaele, L. Fratila-Apacheti, A. Zadpoor, "Substrate curvature as a cue to guide spatiotemporal cell and tissue organization," *Biomaterials*, vol. 232, Feb. 2020.

[6] N. Kostina, S. Blanquer, O. Pop-Georgievski, and C. Rodriguez-Emmenegger, "Zwitterionic Functionalizable Scaffolds with Gyroid Pore Architecture for Tissue Engineering," *Macromol Biosci*, vol. 19, Apr. 2019.

[7] Y. Yang, T. Xu, H. Bei, L. Zhang, C. Tang, M. Zhang, and X. Zhao, "Gaussian curvature-driven direction of cell fate toward osteogenesis with triply periodic minimal surface scaffolds," *PNAS*, vol. 119, Oct. 2022.

[8] F. Verisqa, J. Cha, L. Nguyen, H. Kim, and J. Knowles, "Digital Light Processing 3D Printing of Gyroid Scaffold with Isosorbide-Based Photopolymer for Bone Tissue Engineering," *Biomolecules*, vol. 12, Nov. 2022.

[9] J. Wang, S. Stanic, A. Altun, M. Schwentenwein, and H. Grützmacher, "A highly efficient waterborne photoinitiator for visible-light-induced three-dimensional printing of hydrogels," *Chemical Communications*, vol. 54, Jan. 2018.

[10] H. Zadeh, T. Huber, V. Nock, C. Fee, and D. Clucas, "Complex Geometry Cellulose Hydrogels Using a Direct Casting Method,"*Bioengineering*, vol. 7, Jun. 2020.

[11] L. Zhang, W. Lee, X. Li, Y. Jiang, N. Fang, G. Dai, and Y. Liu, "3D direct printing of mechanical and biocompatible hydrogel metastructures," *Bioactive Materials*, vol. 10, Apr. 2022, pp. 48-55.

[12] W. Tang, A. Das, A. Pegoraro, Y. Han, J. Huang, and M. Guo, "Collective curvature sensing and fluidity in three-dimensional multicellular systems," *Nature Physics*, vol. 18, Nov. 2022, pp. 1371-1378.

[13] L. Han, and S. Che, "An Overview of Materials with Triply Periodic Minimal Surfaces and Related Geometry: From Biological Structures to Self-Assembled Sytems," *Advanced Materials*, vol. 30, Mar. 2018.

[14] C. Chávez-Madero, C, Ceballos-González, M. Samandari, and E. Bolivar, "Using chaotic advection for facile high-throughput fabrication of ordered multilayer micro-and nanostructures: Continuous chaotic printing," *Biofabrication*, Mar. 2020.

[15] M. Li, X. Tian, D. Schreyer, and X. Chen, "Effect of Needle Geometry on Flow Rate and Cell Damage in the Dispensing-Based Biofabrication Process," *AlChE*, Aug. 2011.

[16] M. Flores-Jimenez, R. Fuentes-Aguilar, "Bone Tissue Scaffodls Designed With A Porosity Gradient Based On Triply Periodic Minimal Surfaces Using A Parametric Approach," *2021 43rd Annual International Conference of the IEEE Engineering in Medicina & Biology Society (EMBC)*, 2021, pp. 1209-1212.

[17] M. Ouda, O. Al-Ketan, N. Sreedhar, and H. Arafat, "Novel static mixers based on triply periodic minimal surface (TPMS) architectures," *Journal of Environmental Chemical Engineering*, vol. 8, Oct. 2020.

[18] B. MacCallum, E. Naseri, and A. Ahmadi, "Development of a 3D bioprinting system using a Co-Flow of calcium chloride mist," *Bioprinting*, vol. 20, Mar. 2020.